Determination and modeling of the 3-D gradient refractive indices in crystalline lenses

Derek Y. C. Chan, Jonathan P. Ennis, Barbara K. Pierscionek, and George Smith

A simple method of constructing 3-D gradient refractive-index profiles in crystalline lenses is proposed. The input data are derived from 2-D refraction measurements of rays in the equatorial plane of the lens. In this paper, the isoindicial contours within the lens are modeled as a family of concentric ellipses; however, other physically more appropriate models may also be constructed. This method is illustrated by using it to model the 3-D refractive-index profile of a bovine lens.

I. Introduction

Nondestructive measurements of the refractive properties of optical fibers[1] had been applied to determine the spatial distribution of refractive indices in animal crystalline lenses.[2] This method is based on measuring the total refraction suffered by a light beam as it traverses the lens as a function of the position of the incident beam. The refractive-index profile of the lens and the ray path are related by geometric optics. When the lens cross section has circular symmetry and when the value of the refractive index at the edge of the lens is equal to the refractive index of the surrounding medium (index matched), the solution of the integral equation describing the ray path is relatively straightforward.[1,2] When the lens cross section is elliptical the ray path integral equation can still be solved for the index matched case provided one assumes at the outset that the lens surface is isoindicial and refractive-index contours are concentric ellipses.[3,4] However, it is desirable to derive the refractive-index profile without assuming concentric elliptical index contours in the first case. Moreover, for a variety of reasons, it is not always possible to match the index of the surrounding medium to that of the edge of the lens. As a consequence a further step is necessary to obtain an estimate of the magnitude of the refractive-index mismatch before the lens-index profile can be determined.

We propose a simple method of estimating the refractive-index profile applicable to crystalline lenses which exhibit symmetry about at least one axis. The method is based on taking refraction measurements of rays confined to the equatorial plane which is normal to the axis of symmetry. Thus the problem of deducing the refractive-index profile in the equatorial plane is equivalent to the circularly symmetric problem considered earlier.[1] A formula for estimating the refractive-index mismatch ratio from the measured data is given so that index matching is not required. We also outline a simple model for constructing the 3-D refractive-index profile of a lens using results of a 2-D measurement; other more elaborate models can easily be developed. In Sec. II, we briefly review the appropriate governing equations and point out the difficulties associated with the mismatched case. A simple solution is then offered. In Sec III, we examine the accuracy of our method with synthetic data in the equatorial plane generated using the parabolic profile for which analytic solutions are available. We also demonstrate the utility of our method by using measurements of the refraction properties of a bovine lens in the equatorial plane to construct a 3-D refractive-index model of the lens. This model is then used to predict the refraction of rays confined to the sagittal plane.

The ultimate use of this work is to construct 3-D models of the refractive-index profile of crystalline lenses which have aspheric surfaces. Such models are less restrictive than schematic models of lenses which are only applicable to paraxial analysis. One should note that for some vertebrate lenses, for example, the human lens,[5] the lens cross section in the plane containing the optical axis is significantly nonelliptical. Fortunately, the cross section in the equatorial plane (perpendicular to the optical axis) is circular so that it is possible to use our method to determine the refractive-index profile in this cross section.

All authors are with University of Melbourne, Parkville, Victoria 3052, Australia; D. Y. C. Chan and J. P. Ennis are in the Mathematics Department; the other authors are in the Optometry Department.

Received 2 July 1987.
0003-6935/88/050926-06$02.00/0.

II. Theory

Our intention is to obtain an approximate description of the 3-D refractive-index profile of crystalline lenses using data obtained from 2-D measurements made in the equatorial plane of the lenses. As a first approximation, the anterior and posterior portions of the lens shape may be regarded as generated by rotating ellipses sharing a common major axis but different minor axes about the optic or z axis; see Fig. 1. Consider a refraction experiment in which the ray path is confined within the equatorial plane of the lens. The equatorial plane is the plane $z = 0$ and contains the major axis of the generating ellipse, which we take as the y axis. Since the lens is assumed to have rotational symmetry about the z axis, the spatial variation of the lens refractive index is of the form $n(r,z)$, where $r \equiv \sqrt{x^2 + y^2}$. In the equatorial plane ($z = 0$) the refractive index is only a function of the radial coordinate; that is, the refractive index has the form $n(r)$. We suppress the second argument when $z = 0$. The refraction experiment measures the deflection angle $\psi(y)$ of a light beam as a function of the incident beam position y relative to the axis of symmetry (the z axis); see Fig. 1. From geometric optics, $\psi(y)$ is related to the refractive-index profile $n(r)$ by the equation[1,6]

$$\psi(y) = -2\cos^{-1}(y/\rho) + 2yn_s \int_{r_m}^{\rho} \frac{dr}{r[r^2n^2(r) - y^2n_s^2]^{1/2}}. \quad (1)$$

Here n_s is the refractive index of the surrounding medium, and $n(\rho)$ is the refractive index at the lens boundary which is located at the set of points $(r,z) = (\rho,0)$. The lower limit of the integral r_m is a function of y and is given implicitly by the solution of the equation

$$r_m n_m(r_m) = yn_s. \quad (2)$$

Following Pask[7] we introduce a dimensionless variable ξ and a new function $g(\xi)$ defined by

$$n_s\xi \equiv rn(r), \quad (3)$$

$$n(r) \equiv n(\rho)\exp[g(\xi)], \quad (4)$$

so that Eq. (1) may be written as

$$\psi(y) = 2\{\sin^{-1}(y/\rho) - \sin^{-1}(y/\bar{n}\rho)\} - 2y\int_{y}^{\bar{n}\rho} \frac{d\xi g'(\xi)}{(\xi^2 - y^2)^{1/2}}, \quad (5)$$

with

$$\bar{n} \equiv n(\rho)/n_s \quad (6)$$

being the ratio between the refractive index at the edge of the lens $n(\rho)$ and that of the material surrounding the lens n_s. The experimentally relevant regime for the refractive-index ratio is $\bar{n} \geq 1$. For $\bar{n} = 1$, the index-matched case, the term $\{\ldots\}$ in Eq. (5) vanishes, and the resulting integral equation can be inverted to give[7]

$$g(\xi) = \frac{1}{\pi}\int_{\xi}^{\rho} \frac{dy\psi(y)}{(y^2 - \xi^2)^{1/2}}. \quad (7)$$

This result may be verified by a direct substitution of Eq. (7) into Eq. (5) for $\bar{n} = 1$. Thus, given a set of experimentally determined $\psi(y)$ values, the integral equation (7) can be used to calculate the function $g(\xi)$ as a function of ξ. The refractive-index profile $n(r)$ in the equatorial plane may then be obtained parametrically from Eqs. (3) and (4):

$$r = \xi\exp[-g(\xi)]; \quad (8)$$

$$n(r) = n(\rho)\exp[g(\xi)]; \quad (9)$$

since $n(\rho) = n_s$ for the index-matched case.

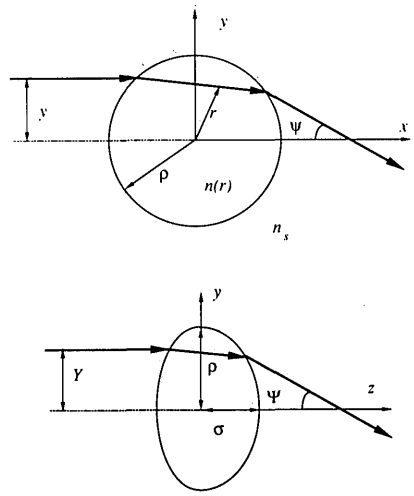

Fig. 1. Schematic diagram of rays in the equatorial (x–y) and sagittal (y–z) planes: y, Y are the beam displacements; ψ Ψ are the emergent angles formed by the beams; n_s is the refractive index of the surrounding medium; ρ is the equatorial; σ is the semiminor axis for the posterior curvature in the illustrated case.

For the mismatched case, $\bar{n} \geq 1$, it is possible to remove the effects of the refraction across the lens boundary due to the index mismatch by transforming the experimentally determined refraction data $[y,\psi(y)]$ into an equivalent set of index-matched data $[\bar{y},\bar{\psi}(\bar{y})]$ given by

$$\bar{y} \equiv y/\bar{n}, \quad (10)$$

$$\bar{\psi} \equiv \psi(y) - 2\{\sin^{-1}(y/\rho) - \sin^{-1}(y/\bar{n}\rho)\}. \quad (11)$$

The data pair $[\bar{y},\bar{\psi}(\bar{y})]$ specifies the position and total deflection of a fictitious ray which entered the lens from an index-matched surrounding: $n_g = n(\rho)$, and has suffered the same amount of deflection within the lens as the ray specified by $[y,\psi(y)]$. As a consequence, the data set $[\bar{y},\bar{\psi}(\bar{y})]$ only contains information about the deflection of the ray within the lens due to the same inhomogeneous refractive-index profile of the lens.

Note that y lies in the range $[0,\rho]$ but $\bar{y}$ is only known over a smaller range $[0,\rho/\bar{n}]$, since $\bar{n} \geq 1$. The physical reason for this is that because of the refraction suffered by the light ray at the boundary of the lens due to the refractive-index mismatch, a portion of the lens near $r \leq \rho$ will not be sampled by the ray. However, we do know that when $\bar{y} = \rho$, $\bar{\psi}(\rho) = 0$ because $[\bar{y},\bar{\psi}(\bar{y})]$ represents a set of index-matched data. Thus the lack of information over the range $[\rho/\bar{n},\rho]$ is not serious as we can interpolate over the range of $\bar{y} = [\rho/\bar{n},\rho]$ if the refractive-index ratio $\bar{n}$ is close to unity. Consequently, we can use the data set $[\bar{y},\bar{\psi}(\bar{y})]$ together with Eqs.

(3), (4), and (7) to construct the refractive-index profile $n(r)$ in the equatorial plane.

The above analysis for the mismatched case assumes that we already know the refractive-index ratio $\bar{n} \equiv n(\rho)/n_s$. In practice, the refractive index of the surround n_s can be readily measured, but a separate experiment is needed to determine the refractive index at the boundary of the lens $n(\rho)$. However, if the index ratio $\bar{n}$ is close to 1, that is, $\bar{n} \equiv 1 + \delta$, where $0 < \delta \ll 1$, it is possible to extract this ratio from the measured refraction data $[y,\psi(y)]$. To do so, we return to Eq. (5) and consider values of $y = [1 - \epsilon]\rho$, where $0 < \epsilon \ll 1$. By expanding the right-hand side of Eq. (5) to leading orders in ϵ and δ we find

$$\psi([1-\epsilon]\rho) = 2\sqrt{2}\{[1 - \rho g'(\rho)]\sqrt{(\epsilon+\delta)} - \sqrt{\epsilon}\} + O(\epsilon^{3/2},\delta^{3/2}). \quad (12)$$

Thus using two data values, $\psi([1 - \epsilon]\rho)$ and $\psi(\rho)$, we can eliminate the unknown quantity $g'(\xi)$ and obtain the following estimate of the refractive-index ratio $\bar{n}$:

$$\bar{n} = 1 + \frac{\epsilon}{(|\psi([1-\epsilon]\rho) + 2\sqrt{2\epsilon}|/\psi(\rho))\lambda^2 - 1}. \quad (13)$$

Note that this extrapolation formula is derived directly from the ray path equation (5) and is independent of the details of the refractive-index profile.

III. Sample Applications

A. Synthetic Data—Parabolic-Index Profile

To test the validity and accuracy of our extrapolation scheme as well as to demonstrate our method of modeling the 3-D refractive-index profile of a lens based on data taken from a 2-D measurement, we use the so-called parabolic-index profile to generate synthetic experimental data for refraction in the equatorial plane. The parabolic-index profile is defined by

$$n(r) = n_0\sqrt{[1 - 2\Delta(r/\rho)^2]}, \quad (14)$$

where n_0 and Δ are constants which characterize the parabolic profile. For this refractive-index profile we have the following exact expression for the refraction angle $\psi(y)$ as a function of the beam position y:

$$\psi(y) = \pi/2 - 2\cos^{-1}(y/\rho) + \sin^{-1}\left\{\frac{1 - 2(1-2\Delta)(y/\bar{n}\rho)^2}{[1 - 8\Delta(1-2\Delta)(y/\bar{n}\rho)^2]^{1/2}}\right\}. \quad (15)$$

B. Refractive-Index Mismatch

In Table I we compare the accuracy of our extrapolation formula of finding the refractive-index mismatch ratio, Eq. (13), for two sets of synthetic parabolic data. As we are interested in applying this work to the analysis of crystalline lenses of various animals, the data set A is chosen so that the refractive-index values at the center and the edge of the lens are comparable with those of bovine lenses. Set B is chosen to illustrate the effects of a large refractive-index mismatch but with a smaller range of variations in the refractive index within the lens. To elucidate the effects of the size of the sampling interval of the deflection angle, we chose ten or twenty equally spaced points of $[y,\psi(y)]$ generated using Eq. (15) over the range $[0,\rho]$ as our input data. These two choices correspond to $\epsilon = 0.1$ or 0.05, respectively. Equation (13) is used to extrapolate for the value of the refractive index $n(\rho)$ at the boundary of the lens. We see from Table I that the formula is accurate even for fairly large values of ϵ and δ. In contrast, if one simply use the value of $\psi(\rho)$ together with the assumption that the refractive index near the lens boundary is approximately constant, the error in the estimated value of $n(\rho)$ would be larger by at least an order of magnitude.

Table I. Input Data Sets for the Parabolic Index Profile [Eq. (14)] and the Extrapolated Refractive Index at the Lens Boundary using Eq. (13) using Ten and Twenty Data Points Corresponding to $\epsilon = 0.1$ and 0.05, Respectively.

	Parabolic index input data			Extrapolated $n(\rho)$	
Set	n_s	$n(0)$	$n(\rho)$	$\epsilon = 0.1$	$\epsilon = 0.05$
A	1.33300	1.42000	1.35000	1.35065	1.35036
B	1.33300	1.45000	1.40000	1.40180	1.40111

C. Refractive-Index Profile in the Equatorial Plane

The extrapolated value of the refractive-index ratio $\bar{n}$ is then used to construct the equivalent index-matched data set $[\bar{y},\bar{\psi}(\bar{y})]$ via Eqs. (10) and (11). The integral in Eq. (7) which connects $[\bar{y},\bar{\psi}(\bar{y})]$ to $[\xi,g(\xi)]$ is calculated by first interpolating between the data points $[\bar{y},\bar{\psi}(\bar{y})]$ using a cubic spline. The integral can then be evaluated once the coeffcients of the spline polynomials are determined. The error in the refractive-index profile in the equatorial plane computed by the method given here is shown in Fig. 2 in terms of the function

$$\Delta n(r) \equiv n^{\text{computed}}(r) - n^{\text{true}}(r). \quad (16)$$

Again we see that the computed values are quite accurate. The errors shown in Fig. 2 are due almost entirely to the error in estimating the refractive-index ratio $\bar{n}$. It is clear, however, that twenty data points are more than sufficient to provide an accurate characterization of the refractive index in the equatorial plane.

Considering the results using ten data points, we see that for $y/\rho \leq 0.8$ the errors for the badly mismatched case [open symbols in Fig. 2(b)] are smaller than that those of the nearly matched case [open symbols in Fig. 2(a)]. The reason for this is that for the badly mismatched data set B, the variation of the refractive index within the lens is over a smaller range than for the nearly matched data set A (see Table I). As the range of the refractive-index variations within a lens increases, the function $\bar{\psi}(\bar{y})$ becomes a more sharply peaked function. Consequently, the interpolation of such a discrete data set by a cubic spline becomes less accurate.

We conclude that provided there is a sufficient number of data points, the algorithm for deducing the refractive-index profile in the equatorial plane is accurate. The two main sources of error in the calculated refractive-index values are in the estimation of the refractive-index ratio $\bar{n}$ and in the range of variations

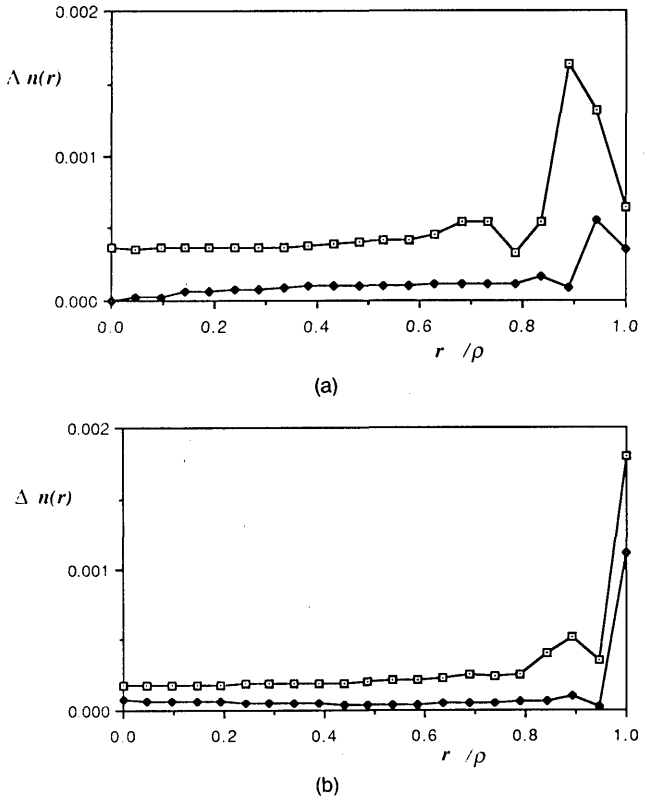

Fig. 2. Error in the computed refractive-index profile $\Delta n(r)$ defined in Eq. (16) for data sets A and B given in Table I: open symbols, ten data points, $\epsilon = 0.1$; solid symbols, twenty data points, $\epsilon = 0.05$.

in the refractive-index profile within the lens. Errors in estimating the refractive-index ratio $\bar{n}$ may be reduced by minimizing the amount of index mismatch in the experimental setup, while the second source of errors may be minimized by taking a sufficient number of sampling points.

D. Three-Dimensional Refractive-Index Profile

Given the form of the refractive-index profile in the equatorial plane $n(r)$, we attempt to model the 3-D distribution of the refractive index $n(r,z)$ of an oblate spheroidal lens whose boundary is generated by rotating the ellipse $(y/\rho)^2 + (z/\sigma)^2 = 1$ about the z axis. (In this case, we assume that the anterior and posterior portions of the lens have the same minor axis.) Here ρ and σ are the semiaxes of the generating ellipse, and we choose an aspect ratio of $\rho/\sigma = 1.6$ (see Fig. 1). We assume that the lens surface is isoindicial, and the refractive-index topography can be generated by rotating a family of concentric elliptical isoindicial contours in the y-z plane about the z axis. In other words, at any point $P = (x,y,z)$ in the interior of the lens we calculate the quantity

$$\alpha^2 \equiv (r/\rho)^2 + (z/\sigma)^2, \qquad r \equiv \sqrt{(x^2 + y^2)}, \tag{17}$$

where $0 \le \alpha^2 \le 1$. The refractive index at P is assigned the value $n(\alpha\rho)$. The refractive-index profile in the equatorial plane for data set A and the index contours

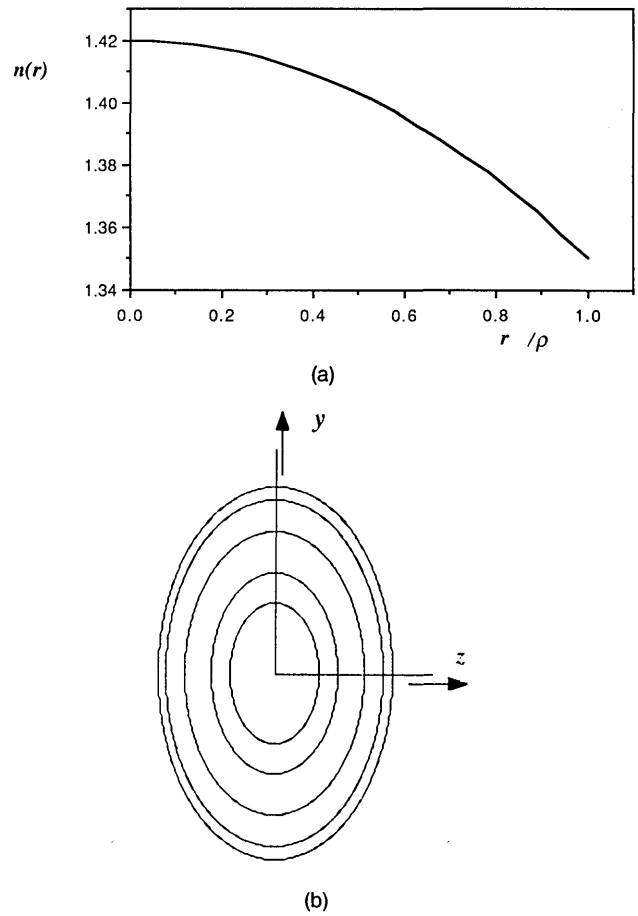

Fig. 3. Equatorial refractive-index profile for data set A and the isoindicial contours of the concentric ellipse model. From the centre to the boundary the refractive-index values on the contours are 1.41, 1.40, 1.38, 1.36, and 1.35 (the lens boundary).

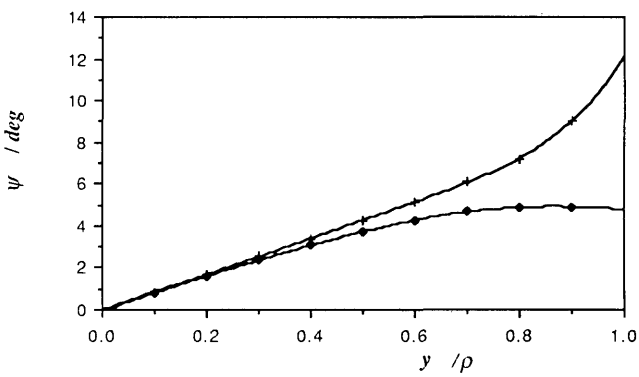

Fig. 4. Deflection angle Ψ (in degrees) as a function of the position (Y/ρ) of incident meridional rays parallel to the z axis: solid symbols, data set A; crosses, data set B.

constructed by this method are illustrated in Fig. 3. The ray tracing results based on such 3-D model lenses for meridional incident rays parallel to the z axis are given in Fig. 4 for both sets of data.

E. Bovine Lens

We also provide some sample results to illustrate that this method can be applied successfully to charac-

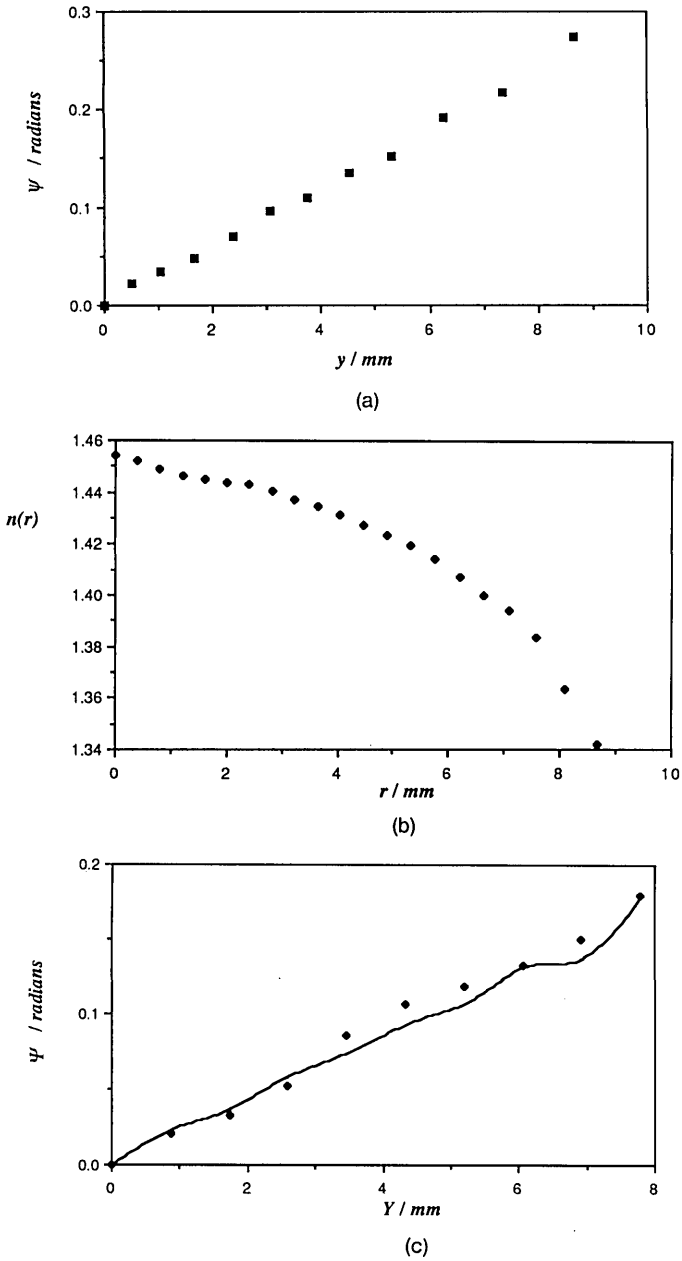

Fig. 5. (a) Experimental measurements of the deflection angle ψ (in radians) as a function of the beam position y for rays in the equatorial plane of a bovine lens. (b) Refractive-index profile $n(r)$ in the equatorial plane deduced from the data in (a). (c) Comparison of the deflection angle angle Ψ (in radians) as a function of beam position Y for rays in the sagittal plane. Points correspond to experimental data, and predicted values based on concentric elliptical isoindicial contours and the results of (b) are given by the continuous line.

terize the optical properties of real crystalline lenses. The experimental data and results summarized in Fig. 5 pertain to a bovine lens weighing 2.07 g. The radius of the lens cross section at the equatorial plane is ρ = 8.65 mm, and the semiaxes of the anterior and posterior portions are 5.83 and 6.75 mm. The experimental data corresponding to a refraction of rays in the equatoril plane are shown in Fig. 5(a). The refractive-index profile in the equatorial plane reduced from this set of data is given in Fig. 5(b). The anterior and posterior surfaces of the lens were modeled as elliptical surfaces, and the 3-D refractive-index profiles in these portions were constructed assuming that the isoindicial surfaces are concentric ellipses. With this model, refraction of rays—traversing from the anterior to the posterior—in the sagittal plane was calculated by standard ray tracing methods; a comparison of the predicted and experimentally measured results is given in Fig. 5(c). Given the simplistic nature of our model and the lack of adjustible parameters, the agreement is very satisfying.

IV. Conclusion

Although general algorithms for reconstructing 3-D refractive-index profiles exist, they are computationally expensive to implement.[8,9] While our reconstruction of the refractive-index profile in the equatorial plane only requires rotational symmetry of the lens about one axis, we need to use a particular model—concentric elliptical-index contours—to describe the 3-D refractive-index profile. However, unlike earlier work,[2] we are not limited to any special model to represent the index profile. A possible elaboration is to allow for the possibility of a family of concentric ellipses with variable degrees of eccentricity. For example, the isoindicial contours near the center of the lens may be more circular than those near the edge of the lens. Also, the anterior and posterior surfaces of crystalline lenses may be better described by ellipses of different eccentricities or indeed by geometric forms other than ellipses. The assumption regarding an isoindicial lens boundary may also be relaxed. The critical test of any gradient-index lens model lies in its ability to predict correctly the fraction of rays that traverse the lens from the anterior to the posterior. Our sample results on bovine lens indicate that our approach does have the desired predictive capacity. A detailed comparison of 3-D gradient-index lens models, which include some of the features discussed above, is given elsewhere.[10]

We thank Colin Pask, Barry Hughes, and Lee White for a number of enlightening discussions. This research is supported by the Australian Research Grants Scheme and the Pank Ophthalmic Trust.

Barbara Pierscionek also works in the Russell Grimwade School of Biochemistry.

References

1. P. L. Chu, "Nondestructive Measurements of Index Profile of an Optical-Fibre Preform," Electron. Lett. 12, 136 (1977).
2. M. C. W. Campbell, "Measurement of Refractive Index in an Intact Crystalline Lens," Vision Res. 24, 409 (1984).
3. K. F. Barrell and C. Pask, "Nondestructive Index Profile Measurement of Non-circular Optical Fibre Preforms," Opt. Commun. 27, 230 (1978).
4. P. L. Chu, "Nondestructive Refractive-Index Profile Measurement of Elliptical Optical Fibre or Preform," Electron. Lett. 15, 357 (1979).

5. M. J. Howcroft and J. A. Parker, "Aspheric Curvatures for the Human Lens," Vision Res. **17**, 1217 (1977).
6. M. Born and E. Wolf, *Principles of Optics* (Pergamon, London, 1975).
7. C. Pask, "The Theory of Non-destructive Lens Index Distribution Measurement," in *Modelling the Eye with Graded Index Optics*, A. Hughes, Ed. (Cambridge U. P., London, 198X) (in press); see also Ref. 2.
8. P. L. Chu and T. Whitbread, "Nondestructive Determination of Refractive Index Profile of an Optical Fiber: Fast Fourier Transform Method," Appl. Opt. **18**, 1117 (1979).
9. P-L. Francois, I. Sasaki, and M. J. Adams, "Practical Three-Dimensional Profiling of Optical Fiber Preforms," IEEE J. Quantum Electron. **18**, 524 (1982).
10. B. K. Pierscionek, D. Y. C. Chan, J. P. Ennis, G. Smith, and R. C. Augusteyn, "A Nondestructive Method of Constructing Three-dimensional Gradient Index Models for Crystalline Lenses: I. Theory and Experiment," Am. J. Optom. Physiol. Optics (in press).

Meetings *continued from page 921*

1988
June

20–22 18th Power Modular Symp., Hilton Head *IEEE, 345 E. 47th St., New York, NY 10017*

20–23 10th Symp. on Thermophysical Properties, Gaithersburg *A. Cezairliyan, Rm. 124 Hazards Bldg., NBS, Gaithersburg, MD 20899*

20–24 14th Int. Laser Radar Conf., San Candido *L. Stefanutti, IROE, CNR, Via Panciatichi, 64-50127 Firenze, Italy*

20–24 Fluid Mechanics Measurement course, Minneapolis *J. Becker, U. of MN, Professional Dev., 107 Armory, 15 Church St. S.E., Minneapolis, MN 55455*

22–24 Medical Laser Safety Officers course, Cincinnati *Laser Inst. Amer., 5151 Monroe St., Toledo, OH 43623*

24–29 5th Conf. Australian Optical Soc., Sydney *AOS Dept. Theoretical Phys., U. Sydney, 2006, Australia*

26–29 Photochemistry for Imaging Symp., Minneapolis *SPSE, 7003 Kilworth Lane, Springfield, VA 22151*

26–30 Engineering & Industrial Sensing for Advanced Manufacturing Technologies Mtg., Dearborn *SPIE, P.O. Box 10, Bellingham, WA 98227*

27–8 July 1st Int. School & Workshop in Photonics, Oaxtepec *J. Ojeda-Castaneda, INAOE, Apdo. Postal 216, 72000 Puebla Pue, Mexico*

July

1–5 4th Ann. Fechner Day Mtg., Edinburgh *H. Ross, Dept. Psychology, U. Stirling, Stirling FK9 4LA, Scotland, U.K.*

11–15 History of Science Soc. & the British Soc. for the History of Science Joint Mtg., Manchester *AIP, 335 E. 45th St., New York, NY 10017*

12–15 Ultrafast Phenomena Top. Mtg., Mt. Hei *Secretariat Ultrafast Phenomena, Opto, Ltd., 5-206 Maeno-cho Heights, 6-10 Maeno-cho, Itabashiku, Tokyo 174, Japan*

18–22 Int. Quantum Electronics Conf., Tokyo *IQEC '88 Secretariat, OITDA, 20th Mori Bldg. 7-4, Nishi-Shimbashi 2-chome, Minato-ku, Tokyo 105, Japan*

19–21 Future of Optical Memories Mtg., San Francisco *TOC, P.O. Box 14817, San Francisco, CA 94114*

25–27 Laser Materials & Laser Spectroscopy Mtg., Shanghai *W. Zhijiang, Topical Mtg. on Laser Materials & Laser Spectroscopy, P.O. Box 8211, Shanghai, China*

25–28 Int. Conf. on Systems Science & Engineering, Beijing *ICSSE'88 Secretariat, Dept. Automation, Tsinghau U., Beijing 100084 China*

25–29 9th Int. Conf. on Spectral Line Shapes, Torun *J. Szudy, Institute of Physics, Nicholas Copernics U., Grudziadzka 5, 87-100 Torun, Poland*

28–30 Optical Fiber Measurements course, Vail *K. Zimmerman, U. Colorado, Boulder, CO 80309*

August

8–12 Non-Ionizing Radiations: Biophysical & Biological Basis, Applications, & Hazards in Medicine & Industry course, Cambridge *Off. of Summer Session, 50 Ames, Rm. E19-356, MIT, Cambridge, MA 02139*

14–19 32nd Ann. Int. Tech. Symp. on Optics & Optoelectronic Appl. Sci. & Eng., San Diego *SPIE, P.O. Box 10, Bellingham, WA 98227*

14–26 34th Scottish Universities Summer School in Physics on Optical Computing, Edinburgh *Dept. Physics, Heriot-Watt U., Edinburgh, Scotland, U.K.*

22–25 **Nonlinear Optical Properties of Materials Top. Mtg.,** Troy *OSA Mtgs. Dept., 1816 Jefferson Pl., NW, Wash., DC 20036*

22–26 4th Int. Conf. on Infrared Phys., Zurich *F. Kneubuhl, Infrared Phys. Lab., IQE, ETH, Hoenggerberg, HPF, CH-8093 Zurich, Switzerland*

28–2 Sept. 18th Int. Congr. on High Speed Photography & Photonics, China *SPIE, P.O. Box 10, Bellingham, WA 98227*

29–1 Sept. Int. Symp. on Applications of Ferroelectrics, Zurich *H. Arends, Lab. Solid State Phys., Swiss Federal Inst. Tech., CH-8093 Zurich, Switzerland*

continued on page 940